

Double parton interactions in γ + 3 jet events in $p\bar{p}$ collisions at $\sqrt{s}=1.96$ TeV in DØ

The DØ Collaboration
URL: http://www-d0.fnal.gov
(Dated: April 24, 2009)

A sample of $\gamma+3$ jet events collected in the D0 experiment with an integrated luminosity of 1 fb⁻¹ is used to determine the fraction of the events with double parton (DP) scattering, $f_{\rm DP}$ in a single $p\bar{p}$ collision at $\sqrt{s}=1.96$ TeV. The events are selected with photon candidate transverse momentum p_T^{γ} within $60 \leq p_T^{\gamma} \leq 80$ GeV, leading jet $p_T > 25$ GeV and two additional jets with $p_T > 15$ GeV. The values of $f_{\rm DP}$ are measured in three intervals of the second jet transverse momentum $p_T^{\rm jet2}$ which spans the range of $15 \leq p_T^{\rm jet2} \leq 30$ GeV. We found that the $f_{\rm DP}$ fractions drop with increasing $p_T^{\rm jet2}$. In the same three $p_T^{\rm jet2}$ intervals, we also calculate an effective cross section $\sigma_{\rm eff}$, a process-independent parameter which contains information about the parton density inside the proton and represents possible parton correlations. The value obtained from averaging over the three $p_T^{\rm jet2}$ intervals is $\sigma_{\rm eff}^{aver}=15.1\pm1.9$ mb.

I. INTRODUCTION

Many features of high energy inelastic hadron collisions depend directly on the parton structure of hadrons which is still not yet well understood at both the theoretical and experimental levels. Phenomenologically, the proton (or antiproton) may be viewed, as an object composed of three light quarks (or anti-quarks). The study of this structure is founded mainly on the use of a simplified theoretical model which considers high energy inelastic scattering of nucleons as a process involving a single collision of one quark or gluon from one nucleon with one quark or gluon from the other nucleon. In this approach, the additional "spectator" partons do not take part in the hard $2 \rightarrow 2$ parton collision and form the so called "underlying event".

Another, much less developed, approach is based on models in which there might be more than one hard interaction of parton pairs in one collision between nucleons. Since each incoming hadron is a composite object, consisting of many partons, such a probability should be non-zero. Models with multiple parton collisions have been considered in a few theoretical papers [1–7]. It is obvious that the rate of events with double parton scattering (DPS) depends on how the partons are distributed within the nucleon. The form of the parton spatial distribution and possible related correlations between partons are practically unknown. This information is hard to obtain within the present theoretical models based on perturbative QCD and makes a relevant measurement particularly important.

To date there have been only four dedicated measurements studying double parton scattering: the AFS experiment in pp collisions at $\sqrt{s}=63$ GeV [8], UA2 in $p\bar{p}$ collisions at $\sqrt{s}=630$ GeV [9] and twice by CDF in $p\bar{p}$ collisions at $\sqrt{s}=1.8$ TeV [10, 11]. The four-jet final state has been used in the first three measurements and the $\gamma+3$ jets final state in the last CDF one to extract values of $\sigma_{\rm eff}$ and $\sigma_{\rm DPS}$ (or $f_{\rm DP}$ fractions). The obtained values of $\sigma_{\rm eff}$ by those experiments are $\sigma_{\rm eff}\sim 5$ mb (AFS), $\sigma_{\rm eff}>8.3$ mb at 95% C.L. (UA2), $\sigma_{\rm eff}=12.1^{+10.7}_{-5.4}$ mb (CDF, four-jet) and $\sigma_{\rm eff}=14.1\pm1.7^{+1.7}_{-2.3}$ mb (CDF, $\gamma+3$ jets).

In the present analysis, we analyse a sample of photon candidate with at least 3 jets events (referred below as " $\gamma + 3$ jets" events) collected by the D0 experiment during Run IIa with an integrated luminosity of 1 fb⁻¹ in $p\bar{p}$ collisions at $\sqrt{s} = 1.96$ TeV to determine the fraction of the double parton interaction in a single $p\bar{p}$ collision and also the value of $\sigma_{\rm eff}$. The latter allows, given the $\gamma + {\rm jets}~\sigma^{\gamma j}$ and dijet σ^{jj} cross sections, the calculation of the $\sigma_{\rm DPS}$ cross section as:

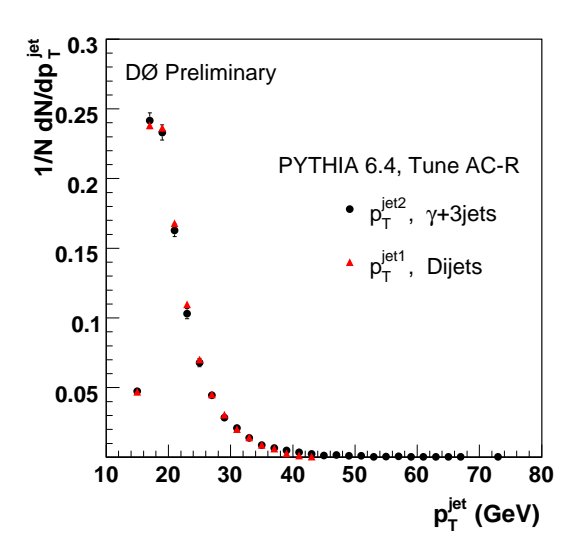
$$\sigma_{DPS} \equiv \frac{\sigma^{\gamma j} \sigma^{jj}}{\sigma_{\text{eff}}} \tag{1}$$

Here the normalization factor σ_{eff} is a parameter that can be directly related to the distance between partons in the nucleon [2, 3, 5, 6, 8–11]. If the partons are uniformly distributed inside the nucleon (large σ_{eff}), σ_{DPS} will be rather low and, conversely, it should grow for a highly concentrated parton spatial densities (small σ_{eff}). A more precise energy measurement of photons as compared to jets helps in separating the DP scatterings and allows us to better fix the scale of the main hard interaction.

In some of the previous analyses with 4-jet final state [8–10], $\sigma_{\rm eff}$ has been calculated from the measured $\sigma_{\rm DPS}$ cross section using QCD predictions for the two dijet cross sections in Eq. (1). A new technique for extracting $\sigma_{\rm eff}$ was proposed in [11]. It operates only with quantities determined from data analysis and minimizes the theoretical assumptions that were used in the previous 4-jet measurements. In the current analysis, we follow this method and extract $\sigma_{\rm eff}$ without any theoretical predictions on the γ + jets and dijets cross sections, by comparing the number of observed DP γ + 3 jets events to the number of γ + 3 jets events with hard interactions occurring in two separate $p\bar{p}$ collisions. The latter class of events will be called double interactions (DI). Assuming independent (uncorrelated) scatterings in the DP process [3, 4], the DP and DI events should be kinematically identical.

The assumption that the additional interaction in the DP events can be considered as independent from the main hard interaction was tested using PYTHIA [12]. In that case, the regular dijet events should describe very well kinematic properties of the second interaction in the DP events. A telling illustration of the independence of the DP interactions could be the p_T and η distributions of the dijet events produced in the $\gamma + 3$ jets DP and regular dijet events. As a model for the DP events, we simulated $\gamma + 3$ jets events without initial and final state radiation but with the MPI model (tune A-CR) turned on $^{(1)}$. This should guarantee that the jets produced in addition to the leading jet in the $\gamma + 3$ jets system are caused by just additional interactions. The regular dijets events were generated without initial

Tune A-CR is usually considered as an example of a model with strong color reconnections and usually give "extreme" predictions for track multiplicities and/or average hadron $p_{\underline{T}}$ (see http://home.fnal.gov/ \sim mskands/leshouches-plots/ and also, for example, Fig. 2 from hep-ph arXiv:0807.3248.)



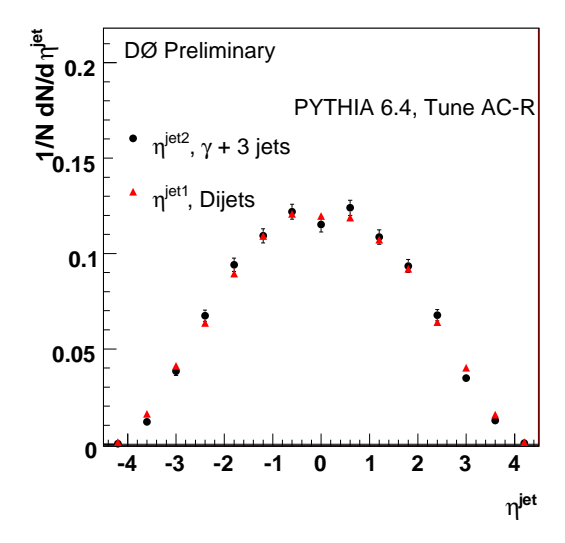


FIG. 1: Difference between the p_T spectra of the second jet in γ + jets events (black circles) and the first jet in the dijet events (red triangles), generated with "tune A-CR" MPI model.

and final state radiation as well, using tune A-CR for the MPI model. The left plot in Fig. 1 compares the p_T spectra of the first jet from DP interaction (second jet in γ + jets events, black circles) and the first jet in the dijet events (red triangles) while right plot compares the η distributions of these jets. We can see a good agreement between kinematics of the second parton interaction and regular dijet events. The same comparison has been done using tunes A and S0 with similar good agreement. Another convincing test of this topic is discussed in the Section V (see the text to Fig. 7).

It was found that single [13] and double [14] diffraction events may give just about 1% contribution to the total dijet production with jet $p_T \gtrsim 15$ GeV. This means that $\gamma + \text{jets}$ and dijet events can be produced as a result of inelastic non-diffractive (hard) $p\bar{p}$ interaction. Then, if we have a $p\bar{p}$ beam crossing with two hard collisions, the probability for a DI event in that crossing is $P_{\text{DI}} = 2 \; (\sigma^{\gamma j}/\sigma_{hard})(\sigma^{jj}/\sigma_{hard})$. Here $\sigma^{jj}/\sigma_{hard}$ (or $\sigma^{\gamma j}/\sigma_{hard}$) is a probability to produce a dijet (or $\gamma + \text{jets}$) event as a separate hard processes. The factor of two takes into account the fact that the two scatterings, producing $\gamma + \text{jets}$ and dijet events, can be ordered in two ways with respect to the two collision vertices. The number of DI events (to first order) can be obtained from P_{DI} , being corrected by the acceptance A_{DI} , the event selection efficiency ϵ_{DI} , the 2-vertex selection efficiency ϵ_{2vtx} , and also multiplied by the number of beam crossings with 2 hard collisions $N_c(2)$:

$$N_{\rm DI} = 2 \frac{\sigma^{\gamma j}}{\sigma_{\rm hard}} \frac{\sigma^{jj}}{\sigma_{\rm hard}} N_c(2) A_{\rm DI} \epsilon_{\rm DI} \epsilon_{2vtx}.$$
 (2)

Analogously to $P_{\rm DI}$, the probability for DP events $P_{\rm DP}$, given a beam crossing with one hard collision, is $P_{\rm DP} = \sigma^{\rm DPS}/\sigma_{\rm hard} = (\sigma^{\gamma j}/\sigma_{\rm eff})(\sigma^{jj}/\sigma_{\rm hard})$ where we used Eq. (1). Then the number of DP events can be expressed from $P_{\rm DP}$ with a correction for the acceptance $A_{\rm DP}$, the event selection efficiency $\epsilon_{\rm DP}$, the 1-vertex selection efficiency $\epsilon_{\rm 1vtx}$, and multiplied by the number of beam crossings with 1 hard collision $N_c(1)$:

$$N_{\rm DP} = \frac{\sigma^{\gamma j}}{\sigma_{\rm eff}} \frac{\sigma^{jj}}{\sigma_{\rm hard}} N_c(1) A_{\rm DP} \epsilon_{\rm DP} \epsilon_{\rm 1vtx}. \tag{3}$$

The ratio of $N_{\rm DP}$ to $N_{\rm DI}$ allows us to obtain the expression for $\sigma_{\rm eff}$ in the following form:

$$\sigma_{\text{eff}} = \frac{N_{\text{DI}}}{N_{\text{DP}}} \frac{N_c(1)}{2N_c(2)} \frac{A_{\text{DP}}}{A_{\text{DI}}} \frac{\epsilon_{\text{DP}}}{\epsilon_{\text{DI}}} \frac{\epsilon_{\text{1vtx}}}{\epsilon_{\text{2vtx}}} \sigma_{\text{hard}}.$$
(4)

It is worth noting that the $\sigma^{\gamma j}$ and σ^{jj} cross sections are reduced in this ratio and that all the remaining efficiencies and acceptances for DP and DI events enter only as ratios.

The main background for the DP events is caused by the $\gamma+3$ jets resulting from single parton (SP) scatterings with hard gluon radiation in the initial or final state $qg \to q\gamma gg$ or $q\bar{q} \to g\gamma gg$. The fraction of DP events is determined in this analysis using a set of variables sensitive to the kinematic configurations of the two independent scatterings of parton pairs (see Sections IV and V).

II. OBJECT IDENTIFICATION

Photon candidates were identified in the DØ detector [15] as isolated clusters of energy depositions in the uranium and liquid-argon sampling calorimeter. The electromagnetic (EM) section of the calorimeter is segmented longitudinally into four layers and transversely into cells in pseudorapidity and azimuthal angle $\Delta \eta \times \Delta \phi = 0.1 \times 0.1$ (0.05 × 0.05 in the third layer of the EM calorimeter). In addition, the cluster may also contain the energy deposited in the hadronic portion of the calorimeter located behind the EM section.

The triggers used in this analysis identify clusters of large electromagnetic energy in events and are based on the photon p_T and loosely on the photon shower shape. These triggers are $\sim 97\,\%$ efficient at $p_T^\gamma \simeq 30$ GeV and are more than 99 % efficient at $p_T^\gamma > 35$ GeV.

To select photon candidates in our data samples, we have used the following criteria [16, 17]. EM objects are reconstructed using a simple cone algorithm with a cone size $\mathcal{R} = \sqrt{(\Delta \eta)^2 + (\Delta \phi)^2} = 0.2$. Central $(|\eta^{\gamma}| < 1)$ and forward $(1.5 < |\eta^{\gamma}| < 2.5)$ photons are considered with $60 < p_T^{\gamma} < 80$ GeV. To avoid inter-calorimeter boundaries and cracks, EM η and ϕ fiducial cuts are applied. Each photon candidate was required to deposit more than 96% of the detected energy in the EM section of the calorimeter (EMfrac > 0.96) and to be isolated in the angular region between $\mathcal{R} = 0.2$ and $\mathcal{R} = 0.4$ around the gravity center of the cluster: $Iso(\Delta \mathcal{R}02) < 0.07$. Here $Iso(\Delta \mathcal{R}02) = (E_{Tot}^{iso} - E_{Core}^{iso})/E_{Core}^{iso}$, where E_{Tot}^{iso} is overall (EM+hadronic) tower energy in the (η, ϕ) circle of radius $\mathcal{R} = 0.4$ and E_{Core}^{iso} is EM tower energy within a radius of $\mathcal{R} = 0.2$. The probability to have any track spatially matched to the EM cluster in the event was required to be below 0.001. We also require the energy-weighted EM cluster width in the finely-segmented EM3 layer to be consistent with that expected for an electromagnetic shower. In addition to the calorimeter isolation, we also apply a track isolation cut, specifically we require the scalar sum of track transverse momenta (p_T^{trk}) in the ring of $0.05 \le \mathcal{R} \le 0.4$ to be less than 1.5 GeV. Only tracks with $p_T^{trk} > 0.4$ GeV are considered.

We also require each event to have at least three jets which are reconstructed using the $\bar{\rm D}\emptyset$ Run II iterative midpoint cone algorithm [18] with a cone size $\mathcal{R}=0.7$. We consider all the jets in the event reconstructed within $|\eta|<3.5$ and require the leading (in p_T) jet to have $p_T^{\rm jet}>25$ GeV, while the next-to-leading jet ("2nd jet") and 3rd jet should have $p_T>15$ GeV.

III. DATA SAMPLES

We used the data collected with the D0 detector during Run IIa, which after applying all the data quality criteria and the trigger selections, corresponds to an integrated luminosity of about 1.02 ± 0.06 fb⁻¹. The EM triggers used in this analysis identify clusters of large electromagnetic energy in events and are based on the photon p_T and loosely on the photon shower shape. These triggers are 100% efficient at $p_T^{\gamma} \simeq 60$ GeV. We consider the following data samples in this analysis.

To determine the fraction of DP events, we select the sample of $\gamma+3$ jets events with the requirement of only one event vertex ("1VTX" sample). The event vertex should have at least three associated tracks and the distance to the center of the detector along the beam axis should be $|z_{vtx}| < 60$ cm. To estimate the fraction of DI events, we also need an additional $\gamma+3$ jets event data sample that differs from the 1VTX sample only by the requirement of two $p\bar{p}$ vertices ("2VTX sample"), each of which should satisfy the same vertex selection criteria as for the 1VTX sample. In both samples, there should be at least one photon candidate and at least 3 jets with criteria described in Section II. Any pair of objects (photon and jets) must be separated in the $\eta-\phi$ space by $\Delta R(\eta,\phi)>0.5$ to avoid photon and/or jets overlapping. To suppress background from $W\to e\nu$ events and cosmics, the missing transverse energy in the event is required to fulfill $E_T^{\rm miss}<0.7$ p_T^{γ} .

We use two models for DP and DI events which are obtained by combining pairs of real events. For the DP model, we mixed 1VTX $\gamma + \geq 1$ jet events and 1VTX minimum bias (MB) events with ≥ 1 jets. The resulting mixed events with jets re-ordered in p_T are also required to have at least one photon candidate and at least three jets with the criteria described above. As we see, the built DP model (called MIXDP) [11] assumes independent scatterings of γ + jets and dijet events by construction.

To build the DI model we exploit the fact that the jets in this sample should originate from separate $p\bar{p}$ collisions. This condition is satisfied by preparing a mixture of $\gamma+\geq 1$ jet events from the 2VTX $\gamma+$ jets data with the 2VTX MB events with ≥ 1 jets. In case of ≥ 2 jets in the MB component of the mixture, the jets are required to originate from the same vertex using the jet tracks information. Similarly to MIXDP, in the mixed events, the jets are re-ordered in p_T and required to pass the $\gamma+3$ jets event selection. We will call this model MIXDI. As a background to the DI events, we also consider the 2VTX $\gamma+3$ jets sample without a hard interaction in the second vertex (BKG2VTX). It was obtained by a direct requirement that all three jets originate from the same vertex using the jet tracks information.

It is worth emphasizing that MIXDP and MIXDI samples differ only by the size of "underlying event" energy that comes from soft interactions in either one or two $p\bar{p}$ collisions. This energy contributes to the jet and photon ID cones

and may change their reconstruction efficiencies. We correct for this difference by calculating $\epsilon_{\rm DI}$ and $\epsilon_{\rm DP}$ efficiencies in Eq. (1).

In this analysis, we estimate the fractions of DP events and then $\sigma_{\rm eff}$ in the three p_T intervals of the second jet $(p_T^{\rm jet2})$, 15–20, 20–25 and 25–30 GeV. All possible event configurations with the $\gamma+3$ jets final state in a single $p\bar{p}$ collision are shown in Fig. 2. The upper diagram (a) shows SP production with a single hard scattering. The bottom diagrams are the signal DP events which may be classified into three types according to the origin of jets. The plot (b) illustrates DP scattering with $\gamma+1$ jet production overlaid with dijet production (Type I). Diagram (c) shows DP scattering with $\gamma+2$ jet production overlaid with dijet production, in which one of the two jets is lost due to jet p_T threshold or finite jet finding efficiency or detector acceptance (Type II). The fraction of the Type I (II) events vary from 23% (75%) at $15 < p_T^{\rm jet2} < 20$ GeV to 14% (86%) at $25 < p_T^{\rm jet2} < 30$ GeV. We also distinguish Type III (diagram (d)) that contains the configuration where a jet from the second interaction becomes the leading jet of the final 3-jets system. This configuration is quite rare and its fraction does not exceed 2%.

Analogous possible event configurations with the $\gamma + 3$ jets final state produced in events with two $p\bar{p}$ collisions are shown in Fig. 3. Plot (a) shows SP production with a hard $p\bar{p}$ collision in one vertex and a soft $p\bar{p}$ collision in the second vertex. The three bottom diagrams show DI production, which can be classified into the three types similarly to the DP ones with about the same fractions in the $p_T^{\rm jet2}$ bins as for DP events.

IV. DISCRIMINATING VARIABLES

A distinctive feature of the DP events is the presence of two independent parton-parton scatterings within the same $p\bar{p}$ collision. To isolate these events in data, we used a collection of variables sensitive to the kinematics of the DP events, specifically to the difference between the p_T imbalances of two pairs in $\gamma + 3$ jets events:

$$S_{p_T} = \frac{1}{\sqrt{2}} \sqrt{\left(\frac{|\vec{p}_T(\gamma, i)|}{\delta p_T(\gamma, i)}\right)^2 + \left(\frac{|\vec{p}_T(j, k)|}{\delta p_T(j, k)}\right)^2}$$
 (5)

$$S_{p_T'} = \frac{1}{\sqrt{2}} \sqrt{\left(\frac{|\vec{p}_T(\gamma, i)|}{|\vec{p}_T^{\gamma}| + |\vec{p}_T^{i}|}\right)^2 + \left(\frac{|\vec{p}_T(j, k)|}{|\vec{p}_T^{j}| + |\vec{p}_T^{k}|}\right)^2}$$
(6)

$$S_{\phi} = \frac{1}{\sqrt{2}} \sqrt{\left(\frac{\Delta\phi(\gamma, i)}{\delta\phi(\gamma, i)}\right)^2 + \left(\frac{\Delta\phi(j, k)}{\delta\phi(j, k)}\right)^2} \tag{7}$$

Variables S_{p_T} , $S_{p_T'}$ have also been used earlier [9–11], while S_{ϕ} is a new one first introduced in this analysis. In the equations above, $\vec{p}_T(\gamma,i)$ and $\vec{p}_T(j,k)$ are the p_T vectors of the total transverse momenta of the two two-body systems, $\Delta\phi(\gamma,i)$ and $\Delta\phi(j,k)$ are the azimuthal angles between them and $\delta p_T(\gamma,i)$, $\delta p_T(j,k)$, $\delta\phi(\gamma,i)$, $\delta\phi(j,k)$ are the corresponding uncertainties. Here uncertainty is RMS of distribution of the related quantity for the signal MIXDP sample. The pairs are constructed by grouping γ with 3 jets in three possible configurations: $(\gamma+jet_1) \oplus (jet_2+jet_3)$, $(\gamma+jet_2) \oplus (jet_1+jet_3)$, and $(\gamma+jet_3) \oplus (jet_1+jet_2)$. The configuration that gives the minimum S is selected for each of the S-family variables. In most events (95-97% in MIXDP sample), S is minimized by pairing the photon with the leading jet, while the additional jets both come from dijet system (Type I) or one of them is replaced by the radiation jet (Type II).

The ΔS -family variables ΔS_{p_T} , $\Delta S_{p_T'}$, and ΔS_{ϕ} are allied to the S-family. They are defined as an azimuthal angle between the p_T vectors of the pairs, $(\gamma + jet_i)$ and $(jet_i + jet_k)$, that give the minimum S:

$$\Delta S = \Delta \phi \left(\mathbf{p}_{\mathrm{T}}^{\gamma, jet_{i}}, \ \mathbf{p}_{\mathrm{T}}^{jet_{j}, jet_{k}} \right)$$
 (8)

Fig. 4 illustrates a possible disposition of the transverse momenta vectors of the photon and jets as well as their p_T imbalances vectors, \mathbf{p}_T^1 and \mathbf{p}_T^2 , in $\gamma + 3$ jets events.

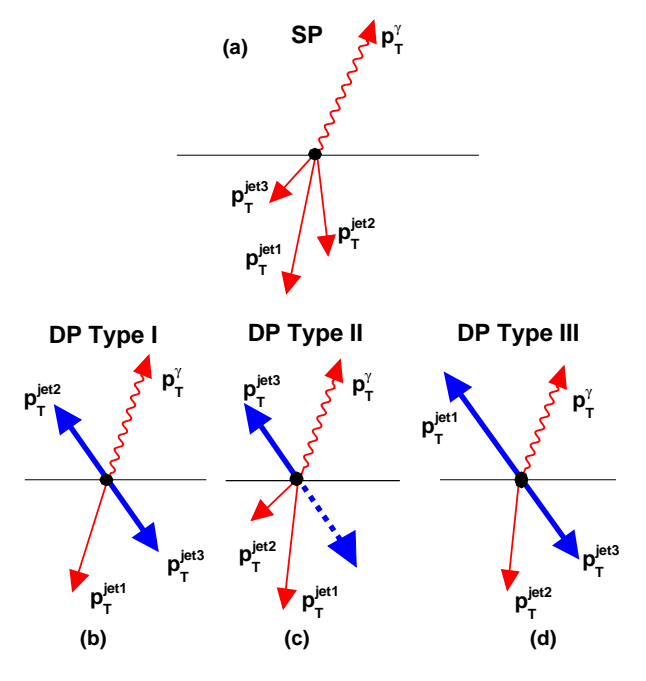


FIG. 2: Diagrams of the $\gamma+3$ jets final state in a single $p\bar{p}$ collision. (a) SP production with a single hard scattering; (b) DP scattering with $\gamma+1$ jet production overlaid with dijet production; (c) DP scattering with $\gamma+2$ jet production overlaid with dijet production, in which one of the two jets is lost; (d) DP scattering with $\gamma+1$ jet production overlaid with dijet production where dijet becomes the leading jet of the final 3-jet system.

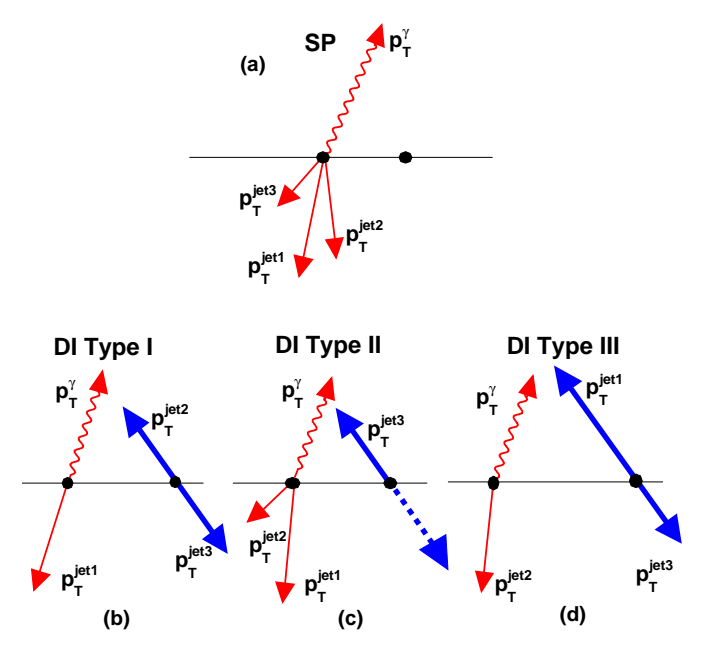


FIG. 3: Diagrams of the $\gamma+3$ jets final state produced in events with two $p\bar{p}$ collisions. (a) SP production in one $p\bar{p}$ collision (vertex) together with an inelastic but soft second collision (vertex); (b) DI production with $\gamma+1$ jet produced in one collision and dijet produced in the second; (c) DI production with $\gamma+2$ jets from one collision and with dijets in the second, but one of the two jets is lost; (d) DI production with $\gamma+1$ jet produced in one collision and dijets produced in the second where dijet becomes the leading jet of the final 3-jet system.

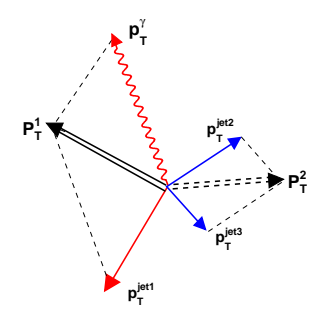


FIG. 4: A possible disposition of photon and jets transverse momenta vectors in $\gamma + 3$ jets events. Vectors p_T^1 and p_T^2 are the p_T imbalance vectors of γ + jets and jet-jet pairs. The figure illustrates a general case for production of the γ + 3 jets +X event.

FRACTIONS OF DP AND DI EVENTS.

Fraction of DP events.

The fraction of the DP events (f_{DP}) is used for the σ_{eff} calculation in (4). To extract this quantity, we use a data driven method and compare distinguishing variables for two sets of the $\gamma + 3$ jets 1VTX data, one of which should contain a larger fraction of the signal events than the other. Since the jet cross section produced in the dijet events drops faster than that of the radiation jets [1, 3], we should expect higher f_{DP} fractions for smaller $p_T^{\rm jet2}$ values. Taking into account two adjacent intervals we can get DP-enriched (e.g. $15 < p_T^{\rm jet2} < 20$ GeV) and DP-depleted (e.g. $20 < p_T^{\rm jet2} < 25$ GeV) samples.

The distribution for each of the distinguishing variable in data can be expressed as a sum of signal (DP) and background (SP) distributions. In particular, for any ΔS -family variable a distribution in data (D) can be expressed as a superposition of MIXDP (M) and background (B) distributions: $D_1 = f_1 M_1 + (1 - f_1) B_1$ and $D_2 = f_2 M_2 + (1 - f_2) B_2$, where f is a fraction of the DP events, (1-f) is a fraction of the SP events, and indices 1 and 2 correspond to the DP-rich and DP-poor data sets. After some transformations we obtain:

$$D_1 - \lambda K D_2 = f_1 M_1 - \lambda K C f_1 M_2 \tag{9}$$

where $\lambda = B_1/B_2$ is a ratio of the background distributions, $K = (1 - f_1)/(1 - f_2)$ is an expected ratio of the SP fractions in the DP-rich and DP-poor samples and $C = f_2/f_1$ is a ratio of the DP fractions in these samples.

The factor λ is extracted as a ratio of ΔS distributions obtained from the SP background samples in the adjacent p_T^{jet2} intervals. We have used γ + jets MC events generated with PYTHIA v6.4 with $\hat{p}_{\perp}^{min}=40$ GeV with the same events selections as for the 1VTX data. We have found that SP events are mostly ($\gtrsim 90\%$ of events) concentrated in the region with $\Delta S > 2.0$ and have very similar ΔS shapes for which λ is about unity. Difference in the shapes is more or less noticeable for events with $\Delta S < 1.5$ with λ varying between 1.1 - 1.3 but here expected fractions of SP events are just 2-4%.

Parameter C is defined here as $C \equiv f_2/f_1 = \left(N_2^{DP}/N_2^{DATA}\right)\left(N_1^{DATA}/N_1^{DP}\right)$ and in particular requires one to determine the ratio N_2^{DP}/N_1^{DP} . The behavior of dijets in events with a single interaction is supposed to be identical to the behavior of dijets in the second hard (DP) interaction (see Section I and Fig. 1). Now, assuming the MIXDP sample correctly models the properties of the DP events, the unknown ratio of the DP events in data can be substituted by the known one from the MIXDP sample: $C = \left(N_2^{MIXDP}/N_2^{DATA}\right)\left(N_1^{DATA}/N_1^{MIXDP}\right)$. Thus, parameter C can be determined without knowledge of the actual amount of DP events in data. We found that $C = 0.694 \pm 0.020$ and 0.701 ± 0.019 for combination of $p_T^{\rm jet2}$ bins 15 - 20/20 - 25 GeV and 20 - 25/25 - 30 GeV, respectively. For extracting the DP fraction in data, we make a χ^2 minimization using MINUIT [19] of this functional form

$$F = |D_1 - f_1 M_1 - \lambda K (D_2 - C f_1 M_2)| / \sigma$$
(10)

for a given distinguishing variable. Parameter σ contains uncertainties on C, D_1, D_2, M_1, M_2 and λ . The only free parameter obtained from the minimization is f_1 . The fit was performed for each pair of $p_T^{\rm jet2}$ bins (15-20/20-25) GeV and 20-25/25-30 GeV) and for each ΔS -family variable. The extracted values of DP fractions are shown in Fig. 5. The DP fractions in the last bin $25 < p_T^{\rm jet2} < 30$ are calculated as $f_2 = Cf_1$. We have studied uncertainties on the f_{DP} fractions by varying λ by 2σ from its central value and found them to be about just 2-3%. Additional uncertainties are caused by varying the number of bins used in the fitting and found to be 3-5%. These two types of uncertainties are added in quadrature to the main uncertainties of the fits. The final DP fractions are summarized in Table I.

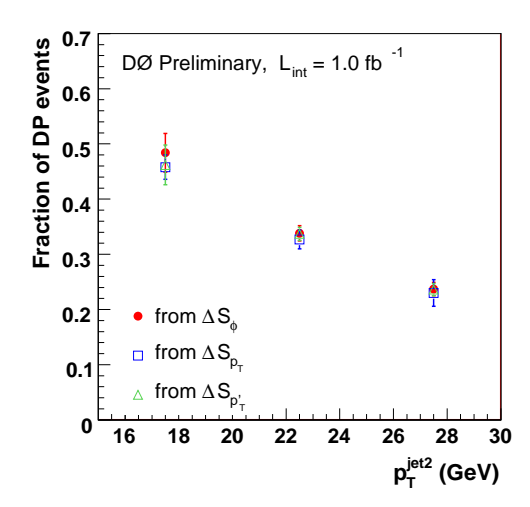


FIG. 5: Fractions of DP events found with ΔS_{ϕ} , ΔS_{p_T} and $\Delta S_{p_T'}$ variables in the four $p_T^{\rm jet2}$ intervals (GeV).

TABLE I: Fractions of DP events $f_{\rm DP}$ found for the three $p_T^{\rm jet2}$ intervals (GeV).

$p_T^{ m je}$	2	15 - 20	20 - 25	25 - 30	
$f_{\rm D}$	Р	0.466 ± 0.041	0.334 ± 0.023	0.235 ± 0.027	

Fig. 6 shows an example of a fit for ΔS_{ϕ} in the combination of bins 15-20/20-25 GeV. Plot (a) shows the distributions for the DP-rich dataset: data (points) and MIXDP (shaded distribution) weighted with its fraction f_1 found from the minimization. Plot (b) shows analogous distributions for the DP-poor dataset: data and MIXDP weighted with $f_2 = Cf_1$. Plot (c) shows the difference of the data distributions in DP-rich and DP-poor datasets corrected for the background contribution (K) and the relative difference of their shapes (λ) (i.e. left side of the Eq.(9)) and DP prediction multiplied by their expected fractions (i.e. right side of the Eq.(9)). One can see that the distributions agree well with each other. From plot (d) we extract SP distributions of the DP-rich and DP-poor dataset by subtracting expected DP fraction from the data: $(D_1 - f_1 M_1)/(1 - f_1)$ (shaded area) for set 1 and $(D_2 - f_2 M_2)/(1 - Cf_2)$ (points) for set 2.

The analogous predictions for SP events were done using PYTHIA. The ΔS distribution for $\gamma+3$ jets jets simulated with initial and final state radiation and without MPI, is shown in Fig. 7. Since the \vec{p}_T imbalance of the two additional jets should compensate the \vec{p}_T imbalance of " $\gamma+$ leading jet" system, the ΔS distribution (black points) reveals a tendency to shift towards π . Comparing this distribution to plot (d) in Fig. 6, one can note a good agreement between them. The DP model was also simulated with PYTHIA without initial and final state radiation but with MPI model (tune A-CR) turned on. In this case, the two additional jets originate from the second interaction (blue triangles), and these $\gamma+3$ jets events correspond to the Type I (see Fig. 2). The ΔS distribution of the DP model is flat, i.e. the two p_T balance vectors for the two systems, $\gamma+$ jets and dijets, "know" nothing about each other, i.e. they are independent from the point of view of this variable.

B. Fraction of DI events.

Similar to DP, we need fraction of the DI events to calculate $\sigma_{\rm eff}$ in (4). Jets in the 2VTX $\gamma+3$ jets events may originate either from the best primary vertex (PV0) or next-to-the-best vertex (PV1). We can distinguish four classes of the events: (I) All three jets originated from PV0 or PV1; (II) Jet1 and Jet2 are from PV0(1) while Jet3 is from PV1(0); (III) Jet1 and Jet3 are from PV0(1) while Jet2 is from PV1(0); (IV) Jet1 is from PV0(1) while Jet2 and Jet3 are from PV1(0). Thus, class (I) corresponds to the $\gamma+3$ jets events in which all three jets come from the same $p\bar{p}$ collision. All other classes (II–IV) correspond to the $\gamma+3$ jets events in which at least one jet come from an additional collision, i.e. we have a double interaction (DI).

The fractions of events in the four classes were first found by the algorithm that exploits information of the charged particles in jets and can determine the jet origin vertex. The algorithm is based on a method which defines the most probable vertex as a vertex containing the highest charged particle fraction (CPF) for a given jet. It requires a jet

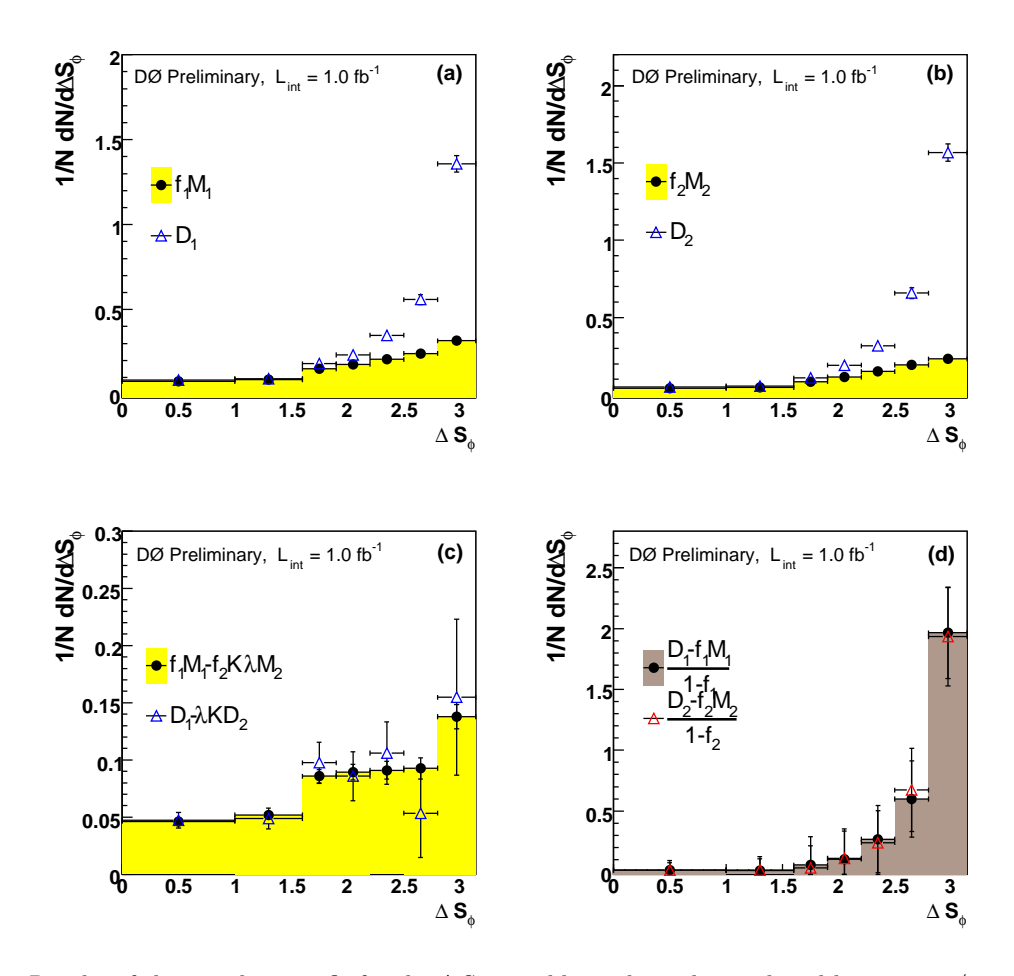


FIG. 6: Results of the two-data-set fit for the ΔS_{ϕ} variable made in the combined bin 15 - 20/20 - 25 GeV.

to have at least two tracks. The fractions of DI events (f_{DI}) found with Jet_cpf algorithm drop from about 24% at $15 < p_T^{\text{jet2}} < 20$ GeV to 15% at $25 < p_T^{\text{jet2}} < 30$ GeV.

Another way to determine the fractions of DI events is based on an application of the ΔS -family variables and three data samples which are the 2VTX data, signal MIXDI, and background BKG2VTX samples. The DI fractions are extracted by fitting the shape of the distribution for a ΔS -family variable in MIXDI and BKG2VTX samples to that in the 2VTX data using minimization [20]. Fig. 8 shows the fractions of DI events found with the ΔS_{ϕ} , ΔS_{p_T} and $\Delta S_{p_T'}$ variables in the three $p_T^{\rm jet2}$ intervals. These fractions are close to those found with the Jet_cpf algorithm and differ from them by a relative error of 4–27%. We took a semi-difference between these DI fractions as our systematic uncertainty in addition to the main uncertainty from the template fitting of the ΔS_{ϕ} , ΔS_{p_T} and $\Delta S_{p_T'}$ distributions in data. The final results on the DI fraction $f_{\rm DI}$ are shown in Table II.

TABLE II: Fractions of DI events f_{DI} found for the three p_T^{jet2} intervals (GeV).

$p_T^{ m jet2}$	15 - 20	20 - 25	25 - 30	
$f_{ m DI}$	0.251 ± 0.029	0.174 ± 0.035	0.115 ± 0.044	

VI. CALCULATING $\sigma_{\rm eff}$

The determination of σ_{eff} is based on expression (4) of Section I that includes the number of DI events N_{DI} , the number of DP events N_{DP} , as well as the efficiencies to satisfy the jet and photon cuts in the DI ε_{DI} and DP ε_{DP}

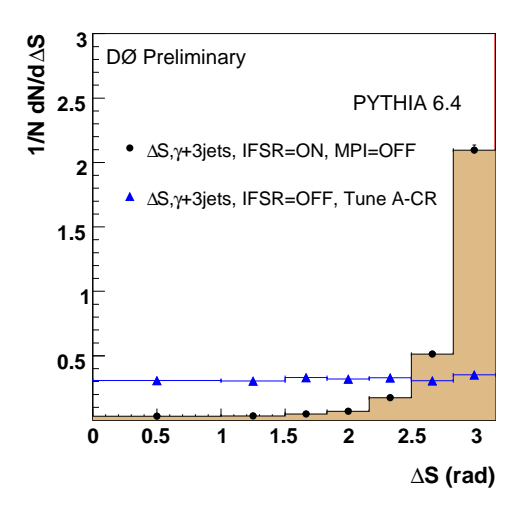


FIG. 7: ΔS distributions for $\gamma + 3$ jets events simulated with ISR/FSR but with MPI switched off (black points), as well as for $\gamma + 3$ jets events without ISR/FSR but MPI switched on using tune A-CR (blue triangles).

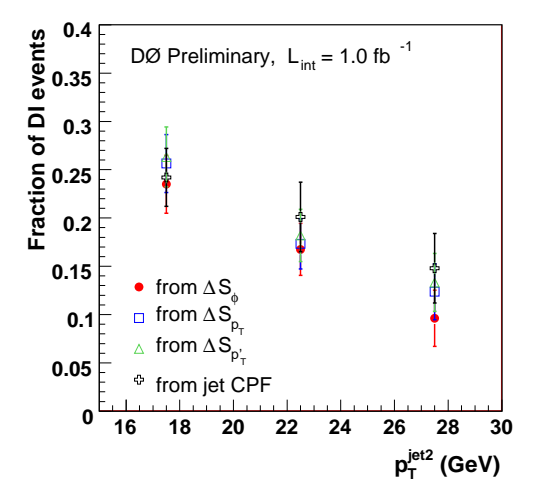


FIG. 8: Fractions of DI events found with the ΔS_{ϕ} , ΔS_{p_T} and $\Delta S_{p_T'}$ variables and "Jet_cpf" algorithm in the four $p_T^{\rm jet2}$ intervals.

events, the efficiencies to get 1-vertex (DP candidate) $\epsilon_{1\text{vtx}}$ and 2-vertex (DI candidate) $\epsilon_{2\text{vtx}}$ events, and finally, the hard $p\bar{p}$ cross section σ_{hard} .

The total number of 1VTX and 2VTX $\gamma + 3$ jets events in the three p_T^{jet2} bins after all our selections is given in Table III. The numbers N_{DI} and N_{DP} in each p_T^{jet2} bin are obtained from them multiplying by fractions of DP and DI events, f_{DP} and f_{DI} , calculated in the previous section.

TABLE III: The numbers of selected 1VTX and 2VTX $\gamma + 3$ jets events in bins of $p_T^{\rm jet2}$.

		$p_T^{ m jet2}~({ m GeV})$				
Sam	ple	15 - 20	20 - 25	25 - 30		
1VT	Ϋ́	2479	3836	3544		
2VT	X	2576	3505	2912		

Let us recall that the only difference between DP and DI events is caused by the number of vertices (1 vs. 2) and

therefore the difference in the $\varepsilon_{\mathrm{DI}}$ and $\varepsilon_{\mathrm{DP}}$ efficiencies come mainly from a different amount of underlying energy in the single and double $p\bar{p}$ collision events. As a result, we can expect different jet reconstruction efficiencies (e.g. different probabilities to pass the jet reco p_T^{raw} cut of 6 GeV, where p_T^{raw} is uncorrected (raw) jet p_T), jet finding efficiencies and jet energy scale. For the photon selection cuts, one can naively expect to get different efficiencies due to, for example, different amount of total p_T in the track and calorimeter isolation cones around the photon.

The efficiencies for the photon selection cuts are initially estimated, using γ + jets MC events generated in PYTHIA [12] with processed through a GEANT-based [24] simulation of the DØ detector and the same reconstruction code as used for the data. Those events are preselected with all our jet and vertex cuts and split into the 1VTX and 2VTX samples which are used to calculate the $\varepsilon_{1\text{vtx}}^{\gamma}$ and $\varepsilon_{2\text{vtx}}^{\gamma}$ efficiencies. We found that the $\varepsilon_{1\text{vtx}}^{\gamma}/\varepsilon_{2\text{vtx}}^{\gamma}$ ratio does not have a noticeable dependence on p_T^{jet2} and can be taken as 0.96 ± 0.03 by averaging over p_T^{jet2} bins. In those estimates, we take into account that photon purity at $60 < p_T^{\gamma} < 80$ GeV in data should be about 75% [16] and assume that the photon purity is same for 1VTX and 2VTX events. To check the latter assumption, we have also analyzed MC dijet events simulated with PYTHIA and calculated how often they pass the photon cuts. We found that the ratio of the photon selection efficiencies for them is 0.99 ± 0.06 . Since this ratio is very close to unity and due to the expected high photon purity, we do not correct the initial $\varepsilon_{1\text{vtx}}^{\gamma}/\varepsilon_{2\text{vtx}}^{\gamma}$ ratio found from the γ + jets events.

The calculation of the ratios of jet efficiencies has been done in two steps. First, they are estimated using a requirement to have at least three jets $(N_{\rm jets} \geq 3)$ with the jet p_T and η cuts described in Section II. The efficiencies have been calculated directly from $\gamma + X$ and dijet (minimum bias) 1VTX and 2VTX events in data using the known fraction of the event types (I, II and III) in MIXDP and MIXDI events (Section III). We found that the ratio of the DP/DI efficiency to pass the cut $N_{\rm jets} \geq 3$ is varied as 0.58 - 0.55 for $p_T^{\rm jet2}$ changing from 15 - 20 GeV to 25 - 30 GeV with a systematic uncertainty of 5.5%. The ratio of all other jet efficiencies (to get into the $p_T^{\rm jet2}$ interval, pass $p_T^{\rm jet3} > 15$ GeV, satisfy geometric acceptance criteria) has been calculated using the MIXDI and MIXDP samples and found to be within 0.95 - 1.03 with about 2% uncertainty.

Taking all the photon and jet efficiencies together, we found that the final ratios of efficiencies in DP to DI events $\varepsilon_{\rm DI}$ / $\varepsilon_{\rm DP}$ in different $p_T^{\rm jet2}$ intervals to range from 0.53-0.57 with relative uncertainty of about 6.5%.

The vertex efficiency corrects for the single (double) collision events that are lost in the DP (DI) candidate sample due to the single (or double) vertex cuts $|z_{vtx}| < 60$ cm and $N_{trk} \ge 3$. The ratio of the $\epsilon_{1\text{vtx}}/\epsilon_{2\text{vtx}}$ vertex efficiencies was calculated from data. We found that this ratio is 1.08 (0.95/0.88) with about 1% uncertainty and does not depend on p_T^{jet2} .

The numbers of the expected single $N_c(1)$ and double $N_c(2)$ $p\bar{p}$ hard collisions can be obtained from the total hard cross section $\sigma_{\rm hard}$ and the instantaneous luminosity L_{inst} for the data sample preselected with a set of EM triggers. For a given instantaneous luminosity, L_{inst} , from the known frequency of beam crossings f_0 for the Tevatron in Run II and $\sigma_{\rm hard}$, we can calculate average number of hard collisions by $\langle n \rangle = (L_{\rm inst}/f_0)\sigma_{\rm hard}$. The value of $\sigma_{\rm hard}$ at $\sqrt{s} = 1.96$ TeV can be obtained from that found at $\sqrt{s} = 1.8$ TeV [11, 21–23] and then extrapolating to 1.96 TeV [25–27]. We found that $\sigma_{\rm hard}$ at $\sqrt{s} = 1.96$ TeV should be 44.76 \pm 2.89 mb. In each bin of the $L_{\rm inst}$ profile, one can get $\langle n \rangle$ and then $N_c(1)$ and $N_c(2)$ can be found from the Poisson distribution. Summing over all the $L_{\rm inst}$ bins, we obtain that $R_c = (1/2)N_c(1)/N_c(2) = 1.169$.

We have to take into account that R_c and $\sigma_{\rm hard}$ enter the formula (4) for $\sigma_{\rm eff}$ as a product. Any increase of $\sigma_{\rm hard}$ leads to an increase of $\langle n \rangle$ and, as a consequence, to a decrease in R_c . And vice versa. Specifically, the found $\sigma_{\rm hard}$ has 6.4% relative uncertainty, while the product $R_c \cdot \sigma_{\rm hard}$ has just about 2% relative uncertainty.

TABLE IV: Effective cross section σ_{eff} (mb) found in the three p_T^{jet2} intervals (GeV).

$\sigma_{ m eff}$	15 - 20	20 - 25	25 - 30	
$p_T^{ m jet2}$	16.2 ± 2.8	13.8 ± 3.1	11.5 ± 4.7	

Now we combine together all the calculations described above and use equation (4) to get $\sigma_{\rm eff}$. The resulting values of $\sigma_{\rm eff}$ with total (systematic \oplus statistics) uncertainties are given in Table V for the three $p_T^{\rm jet2}$ bins and are also shown in Fig. 9. Table V summarizes all the sources of uncertainties for each $p_T^{\rm jet2}$ bin. The impact from jet energy scale (JES) uncertainties was studied by varying the jet p_T within the uncertainties from the JES corrections and recalculation values of $\sigma_{\rm eff}$ after each variation. The total systematic uncertainty varies between 17% and 40% and is mainly caused by the determination of the DI and DP fractions as well as by the ratios of the DP/DI selection efficiencies $\varepsilon_{\rm DI}/\varepsilon_{\rm DP}$.

One can see that the obtained σ_{eff} values in different jet p_T bins agree with each other within their uncertainties. Using this fact and also that the uncertainties in different jet p_T bins have a very small correlation, we can calculate the σ_{eff} value averaged over the three jet p_T bins. It gives us

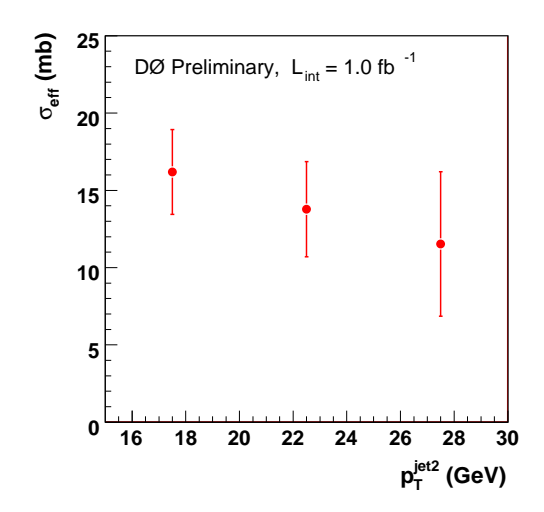


FIG. 9: Effective cross section $\sigma_{\rm eff}$ (mb) measured in the four $p_T^{\rm jet2}$ bins.

TABLE V: Systematic and statistical uncertainties (in %) for σ_{eff} .

	$p_T^{ m jet2}~({ m GeV})$	$f_{ m DP}$	$f_{ m DI}$	$\varepsilon_{ m DI}/\varepsilon_{ m DP}$	JES	$R_c \cdot \sigma_{\mathrm{hard}}$	Syst. Total	Stat. Total	Exp. Total
Γ	15 - 20	8.8	11.5	6.5	5.5	2.0	16.9	2.8	17.1
Γ	20 - 25	6.9	20.0	6.5	2.0	2.0	22.3	2.3	22.5
Ī	25 - 30	11.4	38.2	6.5	3.0	2.0	40.6	2.5	40.6

$$\sigma_{\text{eff}}^{aver.} = 15.1 \pm 1.9 \text{ mb.}$$
 (11)

VII. CONCLUSION.

In the current analysis, we have measured the fractions of the events with double parton scattering $f_{\rm DP}$ in a single $p\bar{p}$ collision in the three intervals of the second jet transverse momentum $p_T^{\rm jet2}$. The results show a decrease of $f_{\rm DP}$ from 0.466 ± 0.041 to 0.235 ± 0.027 with $p_T^{\rm jet2}$ varying from 15-20 GeV to 25-30 GeV. In the same bins of $p_T^{\rm jet2}$ we have also calculated the effective cross sections $\sigma_{\rm eff}$. We found that within uncertainties $\sigma_{\rm eff}$ does not show a dependence on $p_T^{\rm jet2}$ and the averaged value is $\sigma_{\rm eff}^{aver} = 15.1 \pm 1.9$ mb.

It is worth mentioning that the obtained average value is in the range of those found in previous analogous measurements [8–11], what indicates a stable behavior of σ_{eff} with respect to the transverse momentum of the jet produced in the second parton-parton interaction.

^[1] P.V. Landshoff and J.C. Polkinghorne, Phys. Rev. D 18, 3344 (1978);

C. Goebel, F. Halzen, and D.M. Scott, Phys. Rev. D 22, 2789 (1980).

^[2] F. Takagi, Phys. Rev. Lett. 43, 1296 (1979);

N. Paver and D. Treleani, Nuovo Cimento A 70, 215 (1982).

^[3] B. Humpert, Phys. Lett. B 131, 461 (1983);

B. Humpert and R. Odorico, Phys. Lett. B 154, 211 (1985).

^[4] T. Sjöstrand and P.Z. Skands , JHEP 0403, 053 (2004).

^[5] T. Sjöstrand and M. van Zijl, Phys. Rev. D **36**, 2019 (1987).

^[6] G. Calucci and D. Treleani, Nucl. Phys. B (Proc. Suppl.) 71, 392 (1999);

G. Calucci and D. Treleani, Phys. Rev. D 60, 054023 (1999).

^[7] A.M. Snigirev, Phys. Rev. D 68, 114012 (2003);

V.L. Korotkikh and A.M. Snigirev, Phys. Lett. B 594, 171 (2004).

^[8] AFS Collaboration, T. Akesson et al., Z.Phys. C 34, 163 (1987).

- [9] UA2 Collaboration, J. Alitti et al., Phys. Lett. B 268, 145 (1991).
- [10] CDF Collaboration, F. Abe et al., Phys. Rev. D 47, 4857 (1993).
- [11] CDF Collaboration, F. Abe et al., Phys. Rev. D 56, 3811 (1997).
- [12] T. Sjöstrand, Comp. Phys. Comm. 82 74 (1995) 74. Version 6.4 has been used here.
- [13] CDF Collaboration, Phys. Lett. B 531, 52 (2002); Phys. Lett. B 574, 169 (2003).
- [14] D0 Collaboration, Phys. Lett. B 440, 189 (1998).
- [15] D0 Collaboration, V. Abazov et al., Nucl. Instrum. Methods, Phys. Res., A565, 463 (2006).
- [16] D0 Collaboration, V. Abazov et al., Phys. Lett. B 666, 435 (2008).
- [17] D0 Collaboration, V. Abazov et al., arXiv:0901.0739.
- [18] G.C. Blazey et al., arXiv:hep-ex/0005012 (2000).
- [19] F. James, CERN Program Library Long Writeup D506, 1994.
- [20] R. Barlow, C. Beeston, Comp. Phys. Comm. 77, 219 (1993).
- [21] CDF Collaboration, F. Abe et al., Phys. Rev. D **50**, 5550 (1994).
- [22] C. Avila et al., Phys. Lett. B 445, 419 (1999).
- [23] CDF Collaboration, T. Affolder et al., Phys. Rev. Lett. 87, 141802 (2001).
- [24] R. Brun and F. Carminati, CERN Program Library Long Writeup W5013, 1993.
- [25] G.A. Schuler, T. Sjöstrand Phys. Rev. D 49, 2257 (1994).
- [26] A. Capella, J. Tran Thanh Van, J. Kwiecinski, Phys. Rev. Lett. 58, 2015 (1987).
- [27] S. Klimenko, J. Konigsberg, T.M. Liss, Fermilab-FN-0741, 2003.